Science
AAAS

The Last Glacial Maximum

Peter U. Clark, *et al.*

Science **325**, 710 (2009);
DOI: 10.1126/science.1172873

This copy is for your personal, non-commercial use only.

If you wish to distribute this article to others, you can order high-quality copies for your colleagues, clients, or customers by clicking here.

Permission to republish or repurpose articles or portions of articles can be obtained by following the guidelines here.

The following resources related to this article are available online at www.sciencemag.org (this information is current as of May 20, 2010):

Updated information and services, including high-resolution figures, can be found in the online version of this article at:
http://www.sciencemag.org/cgi/content/full/325/5941/710

Supporting Online Material can be found at:
http://www.sciencemag.org/cgi/content/full/325/5941/710/DC1

This article **cites 47 articles**, 21 of which can be accessed for free:
http://www.sciencemag.org/cgi/content/full/325/5941/710#otherarticles

This article has been **cited by** 9 article(s) on the ISI Web of Science.

This article has been **cited by** 2 articles hosted by HighWire Press; see:
http://www.sciencemag.org/cgi/content/full/325/5941/710#otherarticles

This article appears in the following **subject collections**:
Atmospheric Science
http://www.sciencemag.org/cgi/collection/atmos

Downloaded from www.sciencemag.org on May 20, 2010

Science (print ISSN 0036-8075; online ISSN 1095-9203) is published weekly, except the last week in December, by the American Association for the Advancement of Science, 1200 New York Avenue NW, Washington, DC 20005. Copyright 2009 by the American Association for the Advancement of Science; all rights reserved. The title *Science* is a registered trademark of AAAS.

The Last Glacial Maximum

Peter U. Clark,[1]* Arthur S. Dyke,[2] Jeremy D. Shakun,[1] Anders E. Carlson,[3] Jorie Clark,[1] Barbara Wohlfarth,[4] Jerry X. Mitrovica,[5] Steven W. Hostetler,[6] A. Marshall McCabe[7]

We used 5704 ^{14}C, ^{10}Be, and ^{3}He ages that span the interval from 10,000 to 50,000 years ago (10 to 50 ka) to constrain the timing of the Last Glacial Maximum (LGM) in terms of global ice-sheet and mountain-glacier extent. Growth of the ice sheets to their maximum positions occurred between 33.0 and 26.5 ka in response to climate forcing from decreases in northern summer insolation, tropical Pacific sea surface temperatures, and atmospheric CO_2. Nearly all ice sheets were at their LGM positions from 26.5 ka to 19 to 20 ka, corresponding to minima in these forcings. The onset of Northern Hemisphere deglaciation 19 to 20 ka was induced by an increase in northern summer insolation, providing the source for an abrupt rise in sea level. The onset of deglaciation of the West Antarctic Ice Sheet occurred between 14 and 15 ka, consistent with evidence that this was the primary source for an abrupt rise in sea level ~14.5 ka.

The Last Glacial Maximum (LGM) is conventionally defined from sea-level records as the most recent interval in Earth history when global ice sheets reached their maximum integrated volume (*1*). Because sea level is an integrated signal, however, it does not distinguish between globally synchronous ice-sheet maxima that may have been in equilibrium throughout this interval and temporally variable regional ice-sheet maxima that combined to produce a millennia-long sea-level lowstand. Resolving the timing of regional variability in ice-sheet maxima is also important for understanding ice-sheet sensitivity to regional and global climate change, as well as in establishing ice-sheet–climate feedbacks. In particular, key questions that remain widely debated are what initiated the last deglaciation of the global ice sheets and what was their subsequent role during deglaciation in climate change, questions that are best assessed from the record of individual ice sheets rather than the integrated sea-level record.

We drew on 4271 ^{14}C ages and 475 terrestrial cosmogenic nuclide (TCN) ages that span the interval from 10,000 to 50,000 years ago (10 to 50 ka) to constrain the timing of maxima in global ice-sheet extent (Fig. 1). For all but the Barents-Kara and Greenland Ice Sheets, the spatial distribution of ages is sufficient to evaluate regional variability in the timing of maxima for different sectors of individual ice sheets. Because ice-sheet extent scales with ice volume (*2*), our constraints on regional variability in ice-sheet maxima allow us to evaluate the temporal evolution of individual ice-sheet contributions to global sea-level change. Because mountain glaciers are highly sensitive to climate change, we used an additional 172 ^{14}C ages and 786 TCN ages to constrain mountain-glacier fluctuations from five widely distributed regions of the world (Fig. 1), allowing a more comprehensive assessment of the response of the cryosphere to climate change.

The LGM sea-level lowstand. We used existing relative sea level (RSL) data from far-field sites to constrain the timing of the LGM as occurring from 26.5 to 19.0 ka (Fig. 2) (*3*–*5*). The sea-level change at these sites will differ from the eustatic change because of the spatially varying gravitational, deformational, and rotational perturbations in sea level driven by the ice-ocean mass transfer (*6*). In order to evaluate these effects, we used a state-of-the-art theory that includes a realistic glaciation phase to predict the RSL change at these far-field sites (*7*). Our ice model is characterized by a peak eustatic sea-level fall of ~130 m over the LGM (Fig. 2), which is in agreement with independent estimates (*3*, *8*).

We find that in the prediction for Barbados, peripheral bulge dynamics and, to a lesser extent, the continental (lithospheric) levering effect dominate the anti-syphoning effect during the LGM (*7*), leading to a net sea-level fall of ~3 m. In contrast, the remaining four sites lie well outside the peripheral bulges, and the sea-level rise due to anti-syphoning dominates; the net result is a ~4- to 5-m rise in sea level at these sites. Thus, across the LGM period, when the modeled ice history shows no change in the ice volume, the differential sea-level change between Barbados and the other sites approaches 10 m (Fig. 2 and fig. S1).

Global ice-sheet history. Our compilation of radiometric ages suggests that there is considerable regional variability in the timing of when ice sheets (and various sectors of ice sheets) first reached their local last glacial maxima (LLGM) (*9*). Within uncertainties, the earliest maxima were reached by several ice sheets (or sectors of ice sheets) sometime between 29 to 33 ka (Fig. 3B and figs. S2 and S3). This early response included large and small ice sheets at mid- and high northern latitudes, as well as the West Antarctic Ice Sheet (WAIS) in the Southern Hemisphere. Over the next 2500 years, the remaining ice sheets [and sectors of the Laurentide Ice Sheet (LIS)] continued to grow, so that by 26.5 ka, nearly all ice sheets had attained their maximum extents, corresponding to the onset of the LGM sea-level lowstand (Fig. 3C). In the context of the global sea-level record, we find that this expansion of ice sheets to their maximum extent can explain much of the global sea-level fall from intermediate levels during marine isotope stage (MIS) 3 to the LGM lowstand (*7*).

Based on the youngest possible age for ice-sheet maxima derived from our uncertainty assessment (*7*), most of the LIS, the northwest Cordilleran Ice Sheet (CIS), the Barents-Kara Ice Sheet (BKIS), the British-Irish Ice Sheet

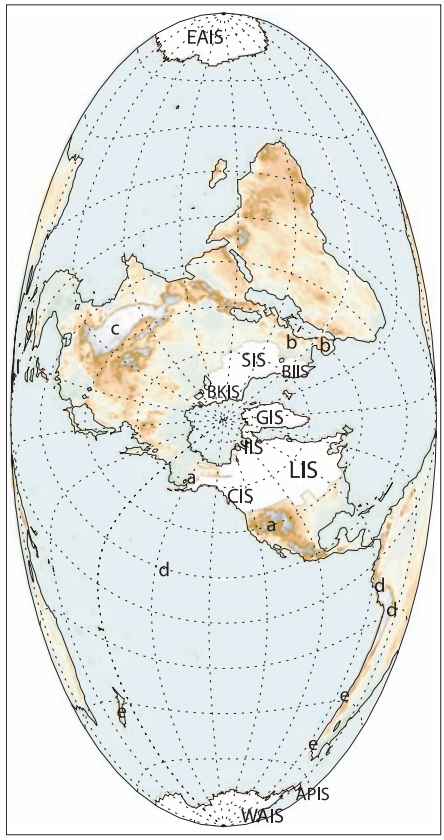


Fig. 1. Distribution of ice sheets at the LGM (*51*). APIS, Antarctic Peninsula Ice Sheet; EAIS, East Antarctic Ice Sheet. Also shown are areas of mountain glaciation discussed in the text (a, western North America; b, Europe; c, Tibet; d, tropics and subtropics; e, Southern Hemisphere).

[1]Department of Geosciences, Oregon State University, Corvallis, OR 97331, USA. [2]Geological Survey of Canada, 601 Booth Street, Ottawa, Ontario K1A 0E8, Canada. [3]Department of Geology and Geophysics, University of Wisconsin, Madison, WI 53706, USA. [4]Department of Geology and Geochemistry, Stockholm University, SE-10691, Stockholm, Sweden. [5]Department of Earth and Planetary Sciences, Harvard University, Cambridge, MA 02138, USA. [6]U.S. Geological Survey, Department of Geosciences, Oregon State University, Corvallis, OR 97331, USA. [7]School of Environmental Science, University of Ulster, Coleraine, County Londonderry, BT52 1SA, UK.

*To whom correspondence should be addressed. E-mail: clarkp@onid.orst.edu

Downloaded from www.sciencemag.org on May 20, 2010

(BIIS), and the Scandinavian Ice Sheet (SIS) had begun to retreat from their maxima between 19 and 20 ka (*10*) (Fig. 3B). Although the onset of Greenland Ice Sheet (GIS) retreat from the LLGM is poorly constrained by existing ^{14}C and TCN ages (fig. S3B), marine records of GIS runoff suggest that GIS retreat may have commenced ~20 ka (*11*). This evidence for widespread ice-margin retreat occurring between 19 and 20 ka indicates that the 19-ka meltwater pulse, which represents a rapid 10-m rise in sea level from the LGM lowstand sometime between 19 and 20 ka (Fig. 3C) (*8*, *12*), originated from these Northern Hemisphere ice sheets (*13*).

In the Southern Hemisphere, the best-dated record from Antarctica is for the WAIS in the Ross Sea region (fig. S3A). Stratigraphic relations of ^{14}C ages to ice-margin history suggest an onset of retreat from the WAIS maximum extent in the Ross Sea between 13.9 and 15.2 ka (*7*) which, within dating uncertainties, corresponds to the rapid rise in sea level ~14.5 ka referred to as meltwater pulse 1A (MWP-1A) (*14*–*19*).

Mountain glaciation. There is information suggesting that in many places, mountain glaciers were near or at their maximum extent by ~30 ka, which is broadly contemporaneous with the interval when global ice sheets first began to reach their maxima (Fig. 3B) (*7*). Within uncertainties (*7*), the TCN-based geochronology suggests that mountain glaciers in western North America, Europe, and the tropics began to retreat from their LLGM positions before those in Tibet and the mid-latitudes of the Southern Hemisphere (Fig. 3A and fig. S4) (*20*–*22*). Moreover, the earlier retreat of Northern Hemisphere mountain glaciers is synchronous, within error, with retreat from most Northern Hemisphere LLGM ice-sheet margins at ~19 ka. The retreat of tropical glaciers may also be synchronous, but because the differences in scaling factors are greatest in the tropics (fig. S4), it is equally likely that tropical-glacier retreat occurred earlier (Fig. 3A).

Discussion and conclusions. We have shown that the duration of the LGM sea-level lowstand (26.5 to 19 ka) is in excellent agreement with the duration of maximum extent of most of the global ice sheets, suggesting that most of the global ice sheets were in near-equilibrium with climate during this 7500-year interval (*23*). We have also documented specific ice-sheet contributions to several key events in the evolution of the integrated global sea-level record into and out of the LGM, including a Northern Hemisphere ice-sheet source for the 19-ka MWP and a significant Antarctic ice-sheet contribution to MWP-1A. Insofar as these two MWP's represent a substantial flux of freshwater into the surrounding ocean, the geographic sources of these events are consistent with inducing the ocean and climate changes that occurred at these times (*12*, *24*).

Our constraints in support of an extended LGM sea-level lowstand provide important insights into the origin of the carbonate $\delta^{18}O$ signal measured in benthic foraminifera ($\delta^{18}O_c$), which is often used directly as a proxy for sea-level change. Disentangling global changes in seawater $\delta^{18}O$ ($\delta^{18}O_{sw}$) from regional changes in seawater temperature ($\delta^{18}O_T$) and water-mass $\delta^{18}O$, however, remains largely unresolved (*25*–*27*), adding considerable uncertainty in interpreting the phase relationship of this proxy to other climate parameters. Comparison of the reasonably well-established global sea-level record for the past 35,000 years (35 ky) (Fig. 4A) with several benthic $\delta^{18}O_c$ records from the Pacific and Atlantic basins (Fig. 4B) clearly demonstrates that the $\delta^{18}O_{sw}$ signal has been compromised by these other effects, and that their relative contribution varies between sites.

We derive a first-order estimate of the $\delta^{18}O_{sw}$ contribution to the global $\delta^{18}O_c$ signal, as represented by the Lisiecki and Raymo (LR04) stack (*28*), by scaling the glacial-interglacial $\delta^{18}O_{sw}$ change of 1.0 ± 0.1 per mil (‰) (*27*) to the corresponding sea-level change of 127.5 ± 7.5 m

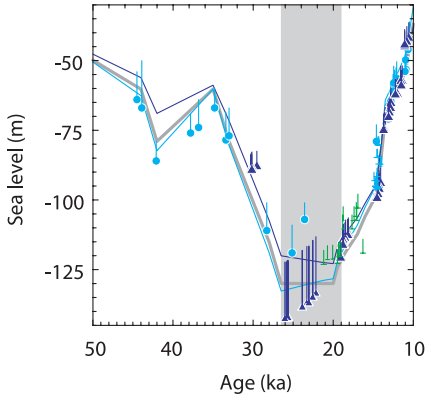


Fig. 2. Sea-level predictions for New Guinea (blue line) and Barbados (purple line) compared to RSL data with depth uncertainty for the interval from 10 to 50 ka from New Guinea (blue circles) (*4*, *52*, *53*), Barbados (purple triangles) (*5*, *54*), the Bonaparte Gulf (green half-pluses representing age and depth uncertainty) (*8*), and the Sunda Shelf (blue half-pluses) (*55*). Eustatic sea-level time series are shown as a gray line. The vertical gray bar indicates the time of the LGM as defined from the RSL data.

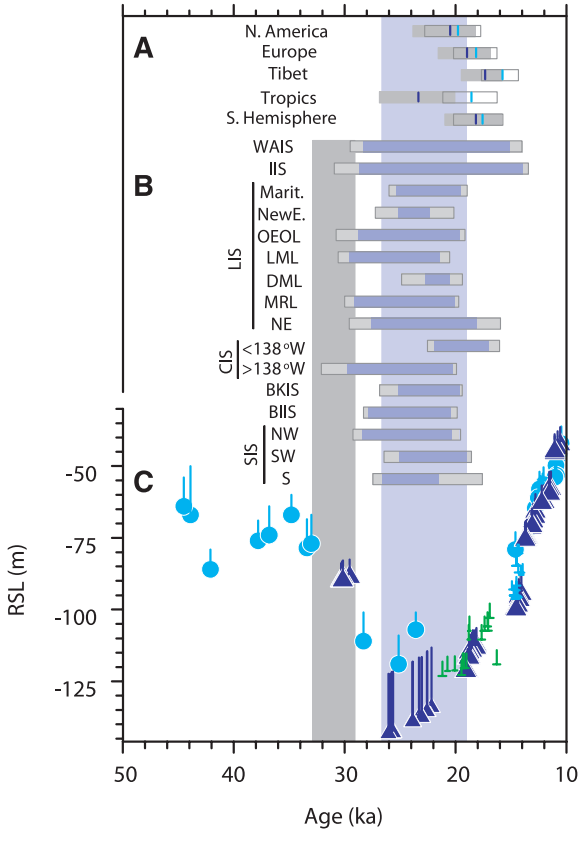


Fig. 3. Summary of glacier and ice-sheet chronologies for LLGM with RSL data constraining the time of the LGM. The vertical purple bar represents the time of the LGM as defined from the RSL data, whereas the vertical gray bar represents the earliest interval when sea level began to fall to the LGM lowstand, corresponding to the time when the first ice-sheet LLGM were reached. (**A**) Summary of the timing of regional deglaciation from the LLGM for the five regions of mountain glaciation evaluated in this paper (small horizontal bars) (fig. S4). In those bars, the vertical purple segment and associated horizontal gray segment represent the mean age and the 1σ age range for the onset of deglaciation based on the scaling factor that delivers the oldest age for the region, whereas the vertical blue segment and associated area outlined in gray represent the mean age and the 1σ age range for the onset of deglaciation based on the scaling factor that delivers the youngest age for the region (*7*). (**B**) Summary of the timing of the LLGM for each of the ice-sheet sectors and ice sheets shown in figs. S2 and S3, with the small horizontal purple bars with gray bars on either end representing the time of the LLGM and associated error, respectively (*7*). The seven LIS sectors are Maritimes (Marit.), New England (NewE.), the Ohio-Erie-Ontario Lobe (OEOL), the Lake Michigan Lobe (LML), the Des Moines Lobe (DML), the Mackenzie River Lobe (MRL), and the northeastern margin (NE). The three SIS sectors are northwest (NW), southwest (SW), and south (S). (**C**) RSL data with depth uncertainty for the interval from 10 to 50 ka from New Guinea (blue circles) (*4*, *52*, *53*), Barbados (purple triangles) (*5*, *54*), the Bonaparte Gulf (green half-pluses representing age and depth uncertainty) (*8*), and the Sunda Shelf (blue half-pluses) (*55*).

Downloaded from www.sciencemag.org on May 20, 2010

(*5*, *8*) (Fig. 4A). In doing so, we adopt ice-sheet model results that suggest that the $\delta^{18}O$ of global ice sheets that contributed to glacial-interglacial sea-level changes was relatively homogenous and thus did not cause any significant temporal changes in this relation (*29*).

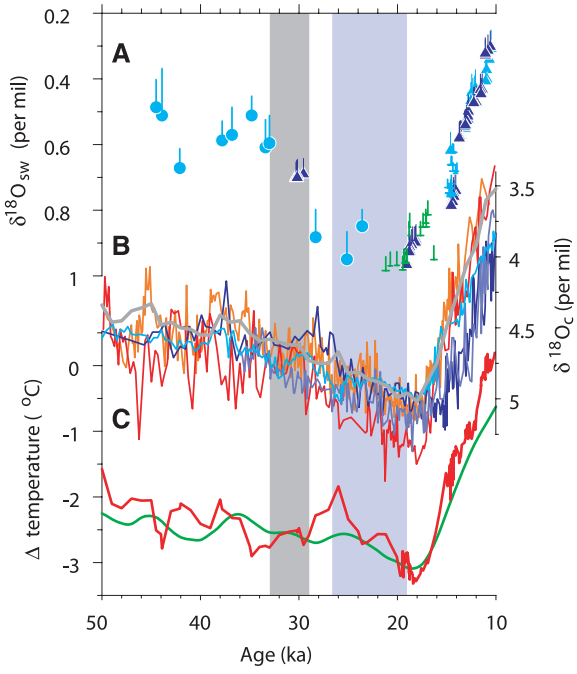


Fig. 4. Constraints on changes in sea level and deep ocean temperature. The vertical purple bar represents the time of LGM as defined from the RSL data, whereas the vertical gray bar represents the earliest interval when sea level began to fall to the LGM lowstand, corresponding to the time when the first ice-sheet LLGM were reached (Fig. 3). (**A**) RSL data for the interval from 10 to 50 ka (Fig. 3), converted to $\delta^{18}O_{sw}$ by scaling the glacial-interglacial $\delta^{18}O_{sw}$ change of 1.0 ± 0.1‰ (*27*) to the corresponding sea-level change of 127.5 ± 7.5 m (*5*, *8*). (**B**) Time series of $\delta^{18}O$ measured in benthic foraminifera from marine cores from the Pacific and North Atlantic basins, as well as the LR04 $\delta^{18}O$ stack (gray line) (*28*). Records are from Pacific core V19-30 (purple line) (*26*), Pacific core TR163-31B (dark purple line) (*25*), Pacific core W8709A-13PC (blue line) (*56*), North Atlantic core NA87-22 (red line) (*26*), and North Atlantic core MD99-2042 (orange line) (*57*). (**C**) The red line shows our estimate of global average deep sea temperature derived by subtracting the sea-level component of seawater in the RSL data (Fig. 4A) from the LR04 benthic $\delta^{18}O$ stack (*28*) (Fig. 4B), with the residual $\delta^{18}O$ converted to temperature using a relation of 0.28‰ $°C^{-1}$. The green line shows the modeled changes in deep ocean temperature from (*29*).

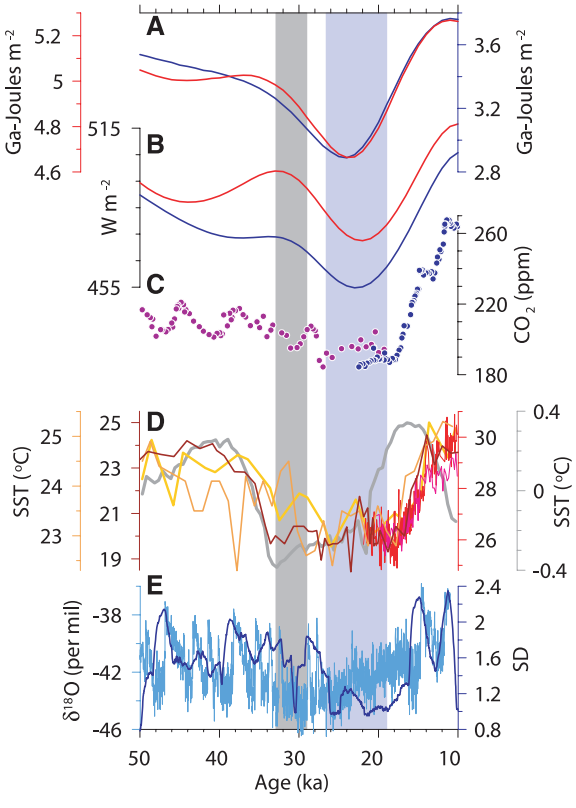


Fig. 5. Temporal relation between the LGM and various climate-forcing factors. The vertical purple bar represents the time of the LGM as defined from the RSL data, whereas the vertical gray bar represents the earliest interval when sea level began to fall to the LGM lowstand, corresponding to the time when the first ice-sheet LLGM were reached (Fig. 3). (**A**) Summer energy for 45°N (red line, $\tau = 400$) and 65°N (purple line, $\tau = 400$). (**B**) 21 June–20 July insolation for 45°N (red line) and 65°N (purple line) (*58*). (**C**) Atmospheric CO_2 from the Dome C ice core (light purple circles) (*59*) and Byrd ice core (dark purple circles) (*60*). (**D**) The 500-year average NINO3 index from the Zebiak-Cane model forced with orbital-scale solar variations (gray line) (*37*) compared to SST records from the tropical Pacific [deep yellow, RC13-110 (*34*); ruby red, ODP 846B (*35*); light orange, TR163-19 (*31*); magenta, MD98-2176 (*40*); red, MD98-2181 (*40*)]. (**E**) The 20-year-resolution $\delta^{18}O$ record from the Greenland NGRIP ice core (*61*) (blue line) and the SD of that record calculated with a centered, 3-ky sliding window (purple line).

We interpret the residual $\delta^{18}O$ signal ($\delta^{18}O_c - \delta^{18}O_{sw}$) as recording the change in mean deep ocean temperature ($\delta^{18}O_T$) (Fig. 4C). Based on a relation of 0.28 ‰ $°C^{-1}$, this analysis suggests a maximum cooling of the mean deep ocean temperature of 3.25 ± 0.55°C, which, for a current mean deep ocean temperature (>2000 m) of 1.3°C (*30*), would place the average temperature of deep ocean waters (–2.2°C) near the freezing point, similar to previous data analyses (*1*, *26*, *27*) and model results (*29*) (Fig. 4C). Within the context of the LGM, however, two additional features of this analysis stand out: Average deep ocean temperatures must have warmed by nearly 1°C during the interval when ice sheets were reaching their maximum extent, followed by a cooling trend through the LGM that culminated in maximum cooling occurring well after the LGM (Fig. 4C). We emphasize that the LR04 stack does not capture regional variability in $\delta^{18}O_T$ and that Skinner and Shackleton (*25*) argued that the Atlantic temperature minimum leads that of the Pacific, as is apparent from the $\delta^{18}O_c$ records shown in Fig. 4B. In contrast, however, these same $\delta^{18}O_c$ records indicate that there are no substantial regional phase offsets in the evolution of temperature leading into and during the LGM, suggesting a more uniform change in the global ocean heat budget during this time.

Our well-established timing of the LGM also allows us to address the forcing mechanisms that induce changes in ice volume and feedbacks with the climate system. Of particular interest is the role that high northern latitude insolation plays in these changes relative to other mechanisms internal to the climate system (*31*, *32*). We focus on three of the more widely proposed mechanisms: high northern latitude insolation, atmospheric CO_2, and tropical Pacific sea surface temperatures (SSTs) (Fig. 5). In evaluating insolation, we include the summer energy index, defined as the sum of insolation at a given latitude on days when a threshold insolation value corresponding to 0°C is exceeded (*33*). Because the relation between temperature and insolation will vary depending on, for example, albedo, elevation, and atmospheric greenhouse gas concentrations, we established the LGM threshold insolation value from an atmospheric general circulation model (AGCM) simulation with glacial boundary conditions (fig. S5) (*7*).

A combination of these three forcing mechanisms appears to explain the growth phase of ice sheets to their LLGM positions. The initial phase of sea-level lowering toward the LGM lowstand, accompanied by the time of earliest LLGM ice-sheet maxima (33 to 29 ka), occurred at the same time that northern summer insolation began to decline (Fig. 5B) and as summer energy was decreasing, particularly at 45°N, where ablation rates along the southern LIS margin would have been most sensitive to this index (Fig. 5A), thus supporting a northern latitude insolation control on ice-sheet growth. This insolation control may have been augmented by additional radiative

Downloaded from www.sciencemag.org on May 20, 2010

forcing from a small (~15 parts per million) decrease in atmospheric CO_2 (Fig. 5C).

There is also a strong temporal relationship between SST changes in the eastern equatorial Pacific and ice growth, which suggests that the 2° to 4°C cooling that occurred between 38 and 30 ka (Fig. 5D) (*31*, *34*, *35*) may have played a role in ice-sheet growth. SST records from the western equatorial Pacific indicate that surface waters in the warm pool had already cooled to LGM values by ~60 ka (*31*, *36*), suggesting that the decrease in SSTs in the eastern equatorial Pacific between 38 and 30 ka reflects a decrease in the equatorial zonal SST gradient, resulting in a more La Niña–like SST field. A model of the response of the NINO3 index (the SST anomaly averaged over 150°W to 90°W and 5°S to 5°N) to orbital forcing indicates that this cooling may have been caused by changes in low-latitude precession-related insolation (*37*) (Fig. 5D).

Regardless of their cause, AGCM simulations show that these changes in tropical Pacific SSTs would have induced a significant increase in the mass balance of Northern Hemisphere ice sheets (*38*) and thus were an important factor in explaining the ice-sheet growth phase. We used these simulations to estimate the possible sea-level response to a cooling of the tropical Pacific. For example, in the case of an intermediate-sized (MIS 3) LIS, cooling of the tropical Pacific induces a mass balance increase of 0.17 m $year^{-1}$ (*38*), which integrated over the area of the ice sheet for 6500 years (33.0 to 26.5 ka) results in a global sea-level fall of ~24 m (*39*). It is likely, however, that as the LIS expanded, the additional ice-sheet area added mass as well. Assuming that a similar mass balance increase (0.17 m $year^{-1}$) applied to the LIS expanding in area at an average rate of 611 km^2 $year^{-1}$ results in a sea-level fall of ~31 m. This analysis thus indicates that tropical Pacific SST cooling probably played an important role in causing the 32 to 38 m of sea-level fall associated with the growth of the LIS to its LLGM extent that we estimated from area-volume scaling relations (*7*). AGCM simulations further show that other Northern Hemisphere ice sheets responded similarly to tropical Pacific cooling (*38*) and may have caused an additional 13 m of sea-level fall in the 6500-year growth interval. The WAIS also reached its LLGM extent early in this growth interval (Fig. 3B), with its growth explaining much of the remaining sea-level fall to the LGM lowstand. In this case, recent analyses have shown that local changes in austral spring insolation control (*40*) or the duration of summer at high southern latitudes (*41*) may have induced climate changes that favored ice-sheet growth.

In contrast to the multiple controls that may have induced ice-sheet growth, our geochronology for the LGM clearly demonstrates that only northern insolation led the termination and was thus the primary mechanism for triggering the onset of Northern Hemisphere deglaciation (Fig. 5). Moreover, the fact that ice sheets of all sizes, as well as Northern Hemisphere mountain glaciers, began to retreat at approximately the same time (19 to 20 ka) (Fig. 3, A and B) suggests that the primary insolation control on initial deglaciation was through increased summer ablation, which can substantially reduce the long response times of large ice sheets by enabling dynamical processes that lead to rapid mass loss. When considering the onset of the LGM, we note that most Northern Hemisphere LGM ice sheets were in equilibrium (mass balance) as long as summer insolation was within 10 W m^{-2} (or 0.2 GJ m^{-2} for summer energy) of the minimum value (Fig. 5). The maximum ice sheets may themselves have reinforced this equilibrium condition by maintaining near-constant freshwater fluxes to the oceans and high albedo and orography, thereby reducing their role in causing climate variability (*42*) (Fig. 5E).

Simulated precessional forcing of tropical SSTs (*37*) suggests that the warming of the eastern tropical Pacific should have occurred 4 to 5 ky earlier than it actually began (Fig. 5D), indicating modulation of the SST response to precession by some other mechanism. Insofar as a key element of this simulated response involves the seasonal position of the Intertropical Convergence Zone (ITCZ) (*37*), one possible mechanism may involve high-latitude cooling induced by expansion of ice sheets and sea ice during the LGM and the effect of this cooling in steepening the pole-to-equator temperature gradient and thus shifting the mean position of the ITCZ (*43*). At the same time, this extratropical forcing associated with glacial boundary conditions may have directly caused cooler tropical SSTs (*44*), thus changing the sensitivity of the tropical Pacific to precessional forcing. In any event, warming of tropical Pacific SSTs did not begin until after 19 ka (Fig. 5D) and thus did not contribute to the termination of the LGM.

The onset of deglaciation of some ice sheets and mountain glaciers from their maxima was delayed until after 19 ka (Fig. 3), suggesting the existence of regional controls on glacier mass balance that modulated their response to insolation (*45*). Dyke and Prest (*46*) attributed the lag of the LLGM of the main body of the CIS with respect to the LLGM of the LIS (Fig. 3B) to atmospheric feedbacks associated with the influence of the growing LIS on the surface mass balance of the CIS and vice versa. Initial retreat of the northeastern LIS margin may have started near 19 ka, but retreat rates through the deglaciation were low (*47*), so that the climatic effects of the lingering ice sheet in this region induced a longer LLGM for the adjacent Inuitian Ice Sheet (IIS). The onset of retreat of the WAIS ~14.5 ka was substantially later than the start of regional warming throughout much of the Southern Hemisphere ~18 to 19 ka (*48*, *49*), and its large contribution to MWP-1A (*19*) suggests a nonlinear response to this warming, perhaps through the collapse of buttressing ice shelves.

Finally, we consider the timing of the LGM retreat of mountain glaciers in Tibet and the Southern Hemisphere, which occurred between 16 and 18 ka (Fig. 3A). One possible explanation for the delayed deglaciation in Tibet is that it was due to the strong influence of the East Asian monsoon, which remained unchanged throughout the LGM until it abruptly weakened ~17.5 ka (*50*). This weakening may have resulted in a reduction in moisture delivered to the glacier, causing a shift to negative mass balance. The initial retreat of Southern Hemisphere mountain glaciers, on the other hand, is consistent with the onset of Southern Hemisphere warming (*21*).

Although the lead-lag relationships established here by the timing of the LGM point to northern latitude insolation as the primary trigger of initial deglaciation of most Northern Hemisphere ice sheets and glaciers, subsequent increases in atmospheric CO_2 and tropical Pacific SSTs (Fig. 5, C and D) demonstrate the importance of carbon cycle and ocean feedbacks in amplifying the deglacial response and causing global warming. Whether these changes in CO_2 and SSTs were induced by deglaciation of Northern Hemisphere ice sheets (*12*) or high southern latitude insolation (*40*, *41*), however, remains an open question.

References and Notes

1. A. C. Mix, E. Bard, R. Schneider, *Quat. Sci. Rev.* **20**, 627 (2001).
2. W. S. B. Paterson, *The Physics of Glaciers: 3rd Edition* (Pergamon, New York, 1994).
3. K. Lambeck, J. Chappell, *Science* **292**, 679 (2001).
4. K. B. Cutler *et al.*, *Earth Planet. Sci. Lett.* **206**, 253 (2003).
5. W. R. Peltier, R. G. Fairbanks, *Quat. Sci. Rev.* **25**, 3322 (2006).
6. G. A. Milne, J. X. Mitrovica, *Quat. Sci. Rev.* **27**, 2292 (2008).
7. Materials and methods are available as supporting material on *Science* Online.
8. Y. Yokoyama, K. Lambeck, P. De Deckker, P. Johnston, L. K. Fifield, *Nature* **406**, 713 (2000).
9. We distinguish the LLGM from the LGM to emphasize the regional variability in the timing of ice-sheet and glacier fluctuations relative to the globally integrated sea-level record used to define the LGM.
10. There is evidence that some ice margins experienced small (tens of kilometers) fluctuations while at or near their LLGM position, such as the New England margin at Martha's Vineyard or the margin of the Ohio-Erie lobe in Ohio (7). We define the termination of the LLGM on the basis of when the margin began a sustained retreat from its LLGM position.
11. A. E. Carlson, J. S. Stoner, J. P. Donnelly, C. Hillaire-Marcel, *Geology* **36**, 359 (2008).
12. P. U. Clark, A. M. McCabe, A. C. Mix, A. J. Weaver, *Science* **304**, 1141 (2004).
13. The CIS and IIS remained at their maxima until after 19 ka. The southern margin of the CIS (where dating constraints are best) retreated from its maximum extent between 16 and 17 ka, whereas the IIS was the last of the global ice sheets to start to retreat from its maximum extent at ~13.5 ka (Fig. 3B).
14. Several additional lines of evidence support a significant change in WAIS volume at this time. The isotopic (δD and $\delta^{18}O$) records from two ice cores bordering the Ross Sea (the Siple and Taylor Domes) show an abrupt warming at 14.5 ka (*15, 16*), which may reflect

Downloaded from www.sciencemag.org on May 20, 2010

ice-surface lowering or some regional climate change induced by ice-surface lowering. If attributed solely to a change in ice-surface elevation, the 3° to 4°C warming at Siple Dome (*16*) would indicate 500 to 650 m of ice-surface lowering, assuming a free atmospheric lapse rate of 6°C per 1000 m. This magnitude of lowering is supported by ice-sheet modeling, which suggests thinning of Siple Dome ice by 350 m between 14 and 15 ka (*17*). Within the large dating uncertainties of dated marine samples, widespread retreat of the Antarctic Peninsula Ice Sheet margin on the continental shelf also occurred at this time (*18*). These lines of direct evidence for WAIS retreat at the time of MWP-1A are consistent with geophysical modeling of the noneustatic component of the sea-level rise during MWP-1A, which suggests a dominant source from Antarctica (*19*).

15. E. J. Steig *et al*., *Science* **282**, 92 (1998).
16. E. J. Brook *et al*., *Quat. Sci. Rev.* **24**, 1333 (2005).
17. S. F. Price, H. Conway, E. D. Waddington, *J. Geophys. Res. Earth Surf.* **112**, F03021 (2007).
18. D. C. Heroy, J. B. Anderson, *Quat. Sci. Rev.* **26**, 3286 (2007).
19. S. E. Bassett, G. A. Milne, J. X. Mitrovica, P. U. Clark, *Science* **309**, 925 (2005).
20. Based on a larger data set, the mean age for regional deglaciation of mid-latitude Southern Hemisphere mountain glaciers (17.7 ka) is not significantly different from the previously reported mean age (17.3 ka), using the same scaling factor (*21*). Nevertheless, the age of regional deglaciation in the mid-latitude Southern Hemisphere is significantly younger than the regional deglaciation age established for LLGM glaciers at northern mid-latitudes (Fig. 3A), a finding counter to the conclusion that deglaciation in the two hemispheres was synchronous (*21*). The source of this disagreement appears to be that Schaefer *et al*. (*21*) identified "outer LGM" and "inner LGM" moraines in any given region, which in western North America are typically 20 to 21 ka and 16.5 to 17.5 ka, respectively (*22*). In these cases, and to be consistent with the concept of LLGM, we used the TCN ages of the "outer" moraines to mark the onset of regional deglaciation from the LLGM, whereas we viewed the "inner" moraines as recording a subsequent millennial-scale ice-margin fluctuation that is unrelated to the termination of the LLGM.
21. J. M. Schaefer *et al*., *Science* **312**, 1510 (2006).
22. J. M. Licciardi, P. U. Clark, E. J. Brook, D. Elmore, P. Sharma, *Geology* **32**, 81 (2004).
23. Heinrich event 2 (H2), which occurred during the LGM ~24 ka, is generally thought to represent an instability of the LIS. In either case, we view H2 as an anomalous and short-lived event with respect to the 7500-year-long LGM interval, during which time ice sheets were otherwise largely in equilibrium with climate.
24. A. J. Weaver, O. Saenko, P. U. Clark, J. X. Mitrovica, *Science* **299**, 1709 (2003).
25. L. C. Skinner, N. J. Shackleton, *Quat. Sci. Rev.* **24**, 571 (2005).
26. C. Waelbroeck *et al*., *Quat. Sci. Rev.* **21**, 295 (2002).
27. D. P. Schrag, G. Hampt, D. W. Murray, *Science* **272**, 1930 (1996).
28. L. Lisiecki, M. E. Raymo, *Paleoceanography* **20**, PA1003 (2005).
29. R. Bintanja, R. S. W. van de Wal, *Nature* **454**, 869 (2008).
30. S. Levitus, *World Ocean Atlas 1994* (U.S. Government Printing Office, Washington, DC, 1994).
31. D. W. Lea, D. K. Pak, H. J. Spero, *Science* **289**, 1719 (2000).
32. J. Imbrie *et al*., *Paleoceanography* **8**, 699 (1993).
33. P. Huybers, *Science* **313**, 508 (2006).
34. M. Feldberg, A. C. Mix, *Paleoceanography* **18**, 10.1029/2001PA000740 (2003).
35. I. Martinez, L. Keigwin, T. T. Barrows, Y. Yokoyama, J. Southon, *Paleoceanography* **18**, PA000877 (2003).
36. L. Stott, C. Poulsen, S. Lund, R. Thunell, *Science* **297**, 222 (2002).
37. A. C. Clement, R. Seager, M. A. Cane, *Paleoceanography* **14**, 441 (1999).
38. P. U. Clark, S. W. Hostetler, N. G. Pisias, A. Schmittner, K. J. Meisner, in *Ocean Circulation: Mechanisms and Impacts*, A. Schmittner, J. Chiang, S. Hemming, Eds. (Geophysical Monograph 173, American Geophysical Union, Washington, DC, 2007), pp. 209–246.
39. To estimate this mass increase, we used the area of the LIS at 13 ka (7.35×10^6 km^2) multiplied by the mass balance increase of 0.17 m year^{-1} over 6500 years, resulting in 24 m of sea-level equivalent. The LIS expanded to its LGM area of 11.63×10^6 km^2 over 6500 years, resulting in an average annual rate of area increase of 611 km^2 year^{-1}. The assumption that the mass balance increase of 0.17 m year^{-1} applied to this expanding area over 6500 years results in an additional 7 m of sea-level equivalent.
40. L. Stott, A. Timmermann, R. Thunell, *Science* **318**, 435 (2007).
41. P. Huybers, G. Denton, *Nat. Geosci.* **1**, 787 (2008).
42. P. U. Clark, R. B. Alley, D. Pollard, *Science* **286**, 1104 (1999).
43. J. C. H. Chiang, C. M. Bitz, *Clim. Dyn.* **25**, 477 (2005).
44. A. B. G. Bush, S. G. H. Philander, *Science* **279**, 1341 (1998).
45. We examined the possibility that the perturbation to the threshold in summer energy (τ) due to LGM boundary conditions (*7*) may have induced a summer energy budget that favored mountain glaciation LLGM at times other than the LGM, but this did not prove to be the case.
46. A. S. Dyke, V. K. Prest, *Geogr. Phys. Quat.* **XLI**, 237 (1987).
47. J. P. Briner, G. H. Miller, P. T. Davis, R. C. Finkel, *Can. J. Earth Sci.* **42**, 67 (2005).
48. K. Pahnke, R. Zahn, H. Elderfield, M. Schulz, *Science* **301**, 948 (2003).
49. T. Blunier, E. J. Brook, *Science* **291**, 109 (2001).
50. Y. J. Wang *et al*., *Science* **294**, 2345 (2001).
51. W. R. Peltier, *Annu. Rev. Earth Planet. Sci.* **32**, 111 (2004).
52. R. L. Edwards *et al*., *Science* **260**, 962 (1993).
53. J. Chappell, *Quat. Sci. Rev.* **21**, 1229 (2002).
54. E. Bard, B. Hamelin, R. G. Fairbanks, A. Zindler, *Nature* **345**, 405 (1990).
55. T. Hanebuth, K. Stattegger, P. M. Grootes, *Science* **288**, 1033 (2000).
56. A. C. Mix *et al*., in *Mechanisms of Global Climate Change at Millennial Time Scales*, P. U. Clark, R. S. Webb, L. D. Keigwin, Eds. (Geophysical Monograph 112, American Geophysical Union, Washington, DC, 1999), pp. 127–148.
57. N. J. Shackleton, M. A. Hall, E. Vincent, *Paleoceanography* **15**, 565 (2000).
58. J. Laskar, P. Robutel, M. Gastineau, A. C. M. Correia, B. Levrard, *Astron. Astrophys.* **428**, 261 (2004).
59. J. Ahn *et al*., *J. Geophys. Res.* **109**, D13305 (2004).
60. J. Ahn, E. J. Brook, *Science* **322**, 83 (2008).
61. A. Svensson *et al*., *Clim. Past* **4**, 47 (2008).
62. The authors thank J. Licciardi, N. Pisias, and an anonymous reviewer for their constructive comments, and J. Bockheim, B. Hall, and P. Huybers for discussions. This work was supported by NSF (P.U.C., J.D.S., A.E.C., and S.W.H.), the Geological Survey of Canada Climate Change Program (A.S.D.), the University of Wisconsin (A.E.C.), the Swedish Nuclear Fuel and Waste Management Co. (B.W.), and the Canadian Institute for Advanced Research (J.X.M.).

Supporting Online Material

www.sciencemag.org/cgi/content/full/325/5941/710/DC1
Materials and Methods
SOM Text
Figs. S1 to S5
References

27 February 2009; accepted 23 June 2009
10.1126/science.1172873

The Genetic Architecture of Maize Flowering Time

Edward S. Buckler,[1,2,3]* James B. Holland,[1,4]* Peter J. Bradbury,[1,2] Charlotte B. Acharya,[2] Patrick J. Brown,[2] Chris Browne,[1,5] Elhan Ersoz,[2] Sherry Flint-Garcia,[1,5] Arturo Garcia,[1,5] Jeffrey C. Glaubitz,[6] Major M. Goodman,[4] Carlos Harjes,[7] Kate Guill,[1,5] Dallas E. Kroon,[2] Sara Larsson,[3] Nicholas K. Lepak,[1,3] Huihui Li,[8,2,9] Sharon E. Mitchell,[2] Gael Pressoir,[2] Jason A. Peiffer,[3] Marco Oropeza Rosas,[4] Torbert R. Rocheford,[10,11] M. Cinta Romay,[2,12] Susan Romero,[2] Stella Salvo,[1,4] Hector Sanchez Villeda,[5,13] H. Sofia da Silva,[10] Qi Sun,[14] Feng Tian,[2] Narasimham Upadyayula,[10] Doreen Ware,[1,15] Heather Yates,[2] Jianming Yu,[16] Zhiwu Zhang,[2] Stephen Kresovich,[2]* Michael D. McMullen[1,5]*

Flowering time is a complex trait that controls adaptation of plants to their local environment in the outcrossing species *Zea mays* (maize). We dissected variation for flowering time with a set of 5000 recombinant inbred lines (maize Nested Association Mapping population, NAM). Nearly a million plants were assayed in eight environments but showed no evidence for any single large-effect quantitative trait loci (QTLs). Instead, we identified evidence for numerous small-effect QTLs shared among families; however, allelic effects differ across founder lines. We identified no individual QTLs at which allelic effects are determined by geographic origin or large effects for epistasis or environmental interactions. Thus, a simple additive model accurately predicts flowering time for maize, in contrast to the genetic architecture observed in the selfing plant species rice and *Arabidopsis*.

The nature of standing genetic variation and its relation to phenotypic variation in plants affects our understanding of evolution (*1*), sustainable agriculture, and preservation of inter- and intraspecific variation in times of environmental change. Maize inbred lines have an average nucleotide diversity in genic regions around 1% (π = 1 to 1.4%) (*2*, *3*),

Downloaded from www.sciencemag.org on May 20, 2010